Journal of Materials Chemistry A

3D graphene interconnected with hollow carbon sphere framework as high performance cathode material for lithium sulfur batteries

Journal:	*Journal of Materials Chemistry A*
Manuscript ID:	TA-ART-02-2015-000897.R1
Article Type:	Paper
Date Submitted by the Author:	09-Apr-2015

Complete List of Authors:	Liu, Shuang; National University of Defense Technology, College of Aeronautics and Materials Engineering Xie, Kai; National University of Defense Technology, Chen, Zhongxue; National University of Defense Technology, Li, Yujie; National University of Defense Technology, Hong, Xiaobin; National University of Defense Technology, Zhou, Liangjun; National University of Defense Technology, Yuan, Junfei; National University of Defense Technology, Xu, Jing; National University of Defense Technology, School of Aerospace Science and Engineering, Zheng, ChunMan; National University of Defense Technology, School of Aerospace Science and Engineering,

3D graphene interconnected with hollow carbon sphere framework as high performance cathode material for lithium sulfur batteries

Shuangke Liu,[a] *Kai Xie,*[a] *Zhongxue Chen,*[a b] *Yujie Li,*[a] *Xiaobin Hong,*[a] *Jing Xu,*[a] *Liangjun Zhou,*[a] *Junfei Yuan*[a] *and Chunman Zheng**[a]

a College of Aerospace Science and Engineering, National University of Defense Technology, Changsha, 410073, China. E-mail: liu_sk@139.com; zhengchunman@hotmail.com
b College of Chemistry and Chemical Engineering, Hunan University, Changsha, 410082, China

Keyword: Lithium sulfur batteries, sulfur cathode, graphene, hollow carbon sphere, high-performance

To better suppress the capaicty decay over cycling and improve the electrical insulation of sulfur cathode of lithium sulfur (Li-S) batteries, we designed a novel three-dimensional graphene interconnected with hollow carbon sphere (3D rGO-HCS) framework as sulfur host. The 3D rGO-HCS nanostructure was first prepared via hydrothermal self-assembly method followed by carbonization and ethching of SiO_2 core, then sulfur was impregnated into the nanostructure by an in-situ solution deposition method to obtain S@rGO-HCS cathode. The as-prepared cathode material delivers a high discharge capacity of ~770 $mAhg^{-1}$ at 4C rate. More importantly, it has a high capacity retention of 93.9% after 100 cycles and demonstrates a low capacity-decay rate of 0.052% per cycle after 400 cycles at 0.5C rate. The superior comprehensive electrochemical performance of the S@rGO-HCS cathode is ascribed to the synergic effects from the 3D graphene-network design, including fast electron and ion transportion, efficient confinement of polysulfide dissolution and shuttling and successfull maintenance of structural integrity.

1.Introduction

In the past decade, lithium sulfur (Li-S) batteries have been paid intensive attentions as the most promising candidate power sources for next generation electric vehicles, due to the high theoretical specific capacity (1672 $mAhg^{-1}$) and energy density (2600 $Whkg^{-1}$) of sulfur, which are several times higher than those of commercial lithium-ion batteries.[1-4] However, some big chanllenges are urgently needed to be addressed for its practical application. The three main problems of sulfur cathode are insulating characteristics of sulfur ($\sigma=5\times10^{-30}$ S cm^{-1} at 25℃), the dissolution and shuttling effect of the long chain lithium polysulfides (Li_2S_n, $4 \leq n < 8$) in liquid electrolytes,[5,6] and the large volume changes during cycling.[7-9]

To overcome this, various methods have been attempted to improve the battery performance of the sulfur cathode, such as combining sufur with conductive polymers,[10-14] building functional carbon interlayers,[15-18] and encapsulating sulfur into various types of carbon materials including carbon nanotubes,[19-24] micro/mesoporous carbon,[25-31] graphene or graphene oxide,[32-42] carbon nanofibers[43-45] and hollow carbon spheres [46-52].

Among these carbon materials, hollow carbon sphere (HCS) has been regarded as an effective sulfur host for improving the transport of electrons and lithium ions between the sulfur and conductive carbon shells as well as minimizing the lithium polysulfide dissolution and shuttling in the electrolyte. N. Jayaprakash[46] et al reported a mesoporous HCS to encapsulate sulfur for execellent cycling performance with a capacity retention of 91% up to 100 cyles, whereas multiple vapor phase infusion process was needed to reach a reletively high sulfur loading of 70wt%. Zhang et al[47] synthesized double-shell hollow carbon spheres (DHCSs) and then impregnated sulfur into the DHCSs, the nanocomposite showed much better cycling stability with a reversible capacity of 690 $mAhg^{-1}$ after 100 cycles, however, the rate

performance is not satisfactory. Guang He et al[49] synthesized a porous HCS and infiltrated with sulfur, by deliberately tailoring the shell porosity, the optimized material has a capacity retention of 89.4% after 100 cycles.

Recently, the graphene with a single-atom thick two-dimensional structure has been widely used in lithium sulfur batteries due to its unique properties, such as high specific surface area, excellent electronic conductivity and good mechanical flexibility.[34-37] Xu et al [34] reported a graphene-encapsulated sulfur (GES) composites with a high sulfur content of 83.3% by in-situ liquid method, which showed both stable cycle capacity and high rate performance. However, it is not easy to load sulfur homogeneously on the graphene due to the self-aggregation and re-stacking of graphene when combined with sulfur by melt diffusion method. In addition, the graphene is not an effective carbon matrix to confine the polysulfide if it was combined with sulfur alone during cycling.[53] For instance, Chen [54] reported a sandwich-type hybrid carbon nanosheets (SCNMM) consisting of graphene and micro/mesoporous carbon layer and Yang [53] synthesized graphene-based layered porous carbon to encapsulate sulfur as Li-S cathode, both composites delivered high rate capacities in a wide voltage range, but obvious capacity decay could be observed after only 100 cycles.

On the basis of the analysis above, if a nanostructure combining graphene with HCS was built, it may not only offer fast electron/ion transportion and efficient confinement of polysulfide dissolution and shuttling, but also bring up new peculiarities such as 3D conductive networks, flexible mechanical scaffold and hierarchical porous structure. Such nanostructure designing may effectively improve the electrochemical performance of the sulfur cathode material.

Here, we present a rational design and preparation of a novel 3D carbon-network with interlinked connections of graphene sheet and hollow carbon sphere (3D rGO-HCS) with

hierarchical porous structure as the host for sulfur cathode.The HCS with diameter of ~180nm connected uniformly with the 3D graphene networks, the sulfur is highly dispersed into the nanostructure by an in-situ solution deposition method to obtain S@rGO-HCS nanocomposite in liquid environment. In this architecture, the 3D interlinked graphene networks mainly act as the fast electronic conductive channels and flexible mechanical scaffold, while the HCSs mainly act as polysulfide reservoir and volume expansion buffer. Furthermore, the 3D S@rGO-HCS nanostructure with homogeneously distributed nano sulfur can effectively resist the stress from volume expansion and preserve the integrity of the electrode during long cycling. When used as Li-S cathode material, the 3D S@rGO-HCS nanocomposite shows superior comprehensive battery performance, including high rate capacity (~770mAhg-1 at 4C rate), long cycling stability (low capacity decay rate of ~0.052% per cycle for 400 cycles), and excellent Coulombic effecieny (~98% up to 400 cycles).

2 Results and Disscusions

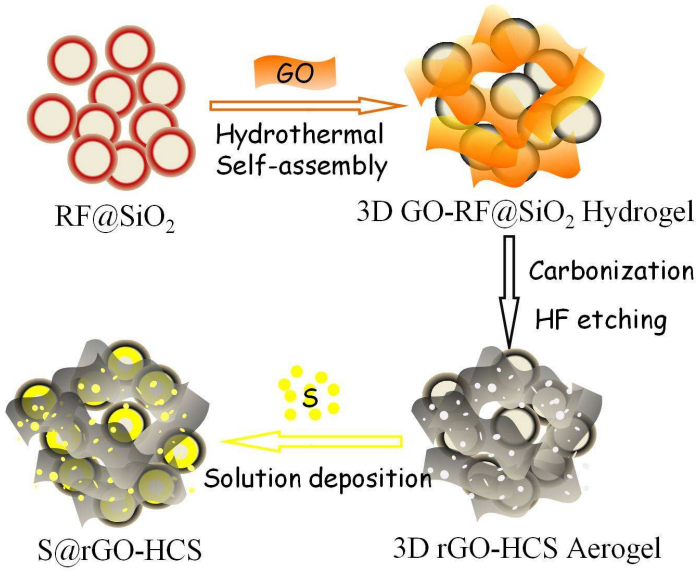

Figure 1 Schematic illustration of the process for preparing S@rGO-HCS nanocomposite

Figure 1 shows the typical process for preparing the S@rGO-HCS nanocomposite, it was

fabricated via a multi-step method using graphene oxide (GO) and resorcinol-formaldehyde@silica (RF@SiO_2) spheres as precusors. The RF@SiO_2 spheres and GO (experimental section) were ultrasonicated in water and mixed well together to form a stable aqueous suspension, then the suspension was hydrothermally treated with the the existing of ascorbic acid as reducing agent to form 3D GO-RF@SiO_2 hydrogel (**Figure S1b**). In this way, the GO and RF@SiO_2 spheres both could be easily dispered well in water, and during hydrothermal condition, the functional groups on the surface of the RF resin and GO will polymerize and the GO sheets will self-assemble to form 3D hydrogel via π-π stacking interactions, during which the reduced GO sheets will interlink evenly with RF@SiO_2 spheres to generate a homogeneous graphene-based 3D hydrogel. Subsequently, the obtained hydrogel was carbonized at high temperature to form a 3D aerogel followed by HF solution etching to remove SiO_2 core, the 3D rGO-HCS nanocomposite (**Figure S1c**) was collected after drying at 100°C. The presence of the RF@SiO_2 spheres among the graphene networks could effectively prevent from the re-stacking of the thin graphene sheets during calcination process and maintain the 3D hybrid nanostructure, the HF etching will introduce nanopores [53] on the surface of graphene and HCS. This method also provide an easy way to prepare 3D rGO-HCS hybrid nanostructure with hierarchical porous structure. The sulfur was impregnated into the 3D rGO-HCS framework by an in-situ precipitation method and ultrasonication treatment (see experimental section), the chemical equation of the precipitation can be draw as:

$2Na_2S + Na_2SO_3 + 6HCl \rightarrow 3S\downarrow + 6NaCl + 3H_2O$

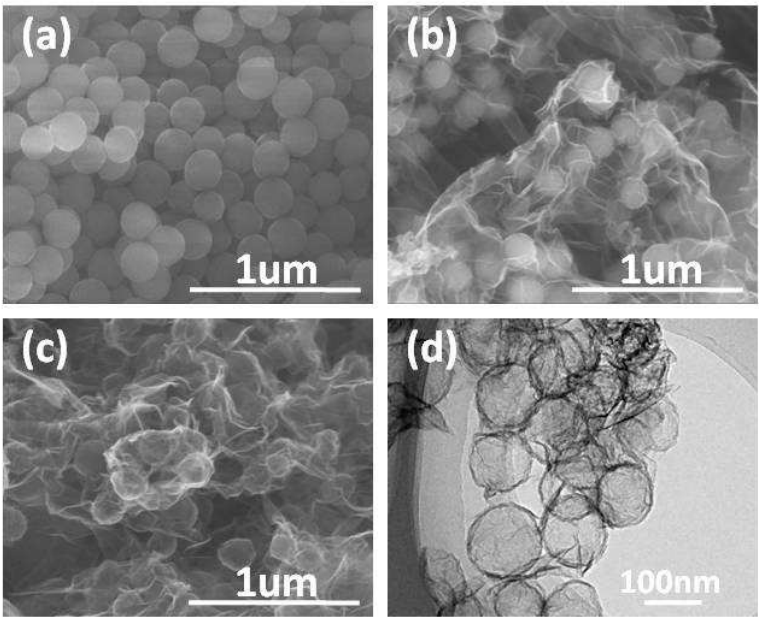

Figure 2 SEM images of (a) RF@SiO_2 spheres,(b)3D GO-RF@SiO_2 gel,(c)3D rGO-HCS nanocomposite and (d) TEM image of 3D rGO-HCS nanocomposite

Figure 2 show the typical field-emission scanning electron microscopy (FESEM) images of the RF@SiO_2 spheres, 3D GO-RF@SiO_2 gel, 3D rGO-HCS nanocomposite and transmission electron microscopy (TEM) of 3D rGO-HCS nanocomposite. As show in Figure 2a, the well-defined RF@SiO_2 nanospheres show uniform diameters of about 200 nm with smooth surfaces. **Figure 2b** shows the nanostructure of 3D GO-RF@SiO_2 hydrogel, the RF@SiO_2 nanospheres disperse loosely among the crumpled graphene networks, clearly demonstrating the separation role of the RF@SiO_2 spheres as nano-spacer of graphene sheets. **Figure2c** demonstrates typical nanostructure of the 3D rGO-HCS nanocomposite, in which HCS derived after carbonization and HF etching interconnected within thin graphene network. The HCS has a shrinked diameter of about 180nm compared to RF@SiO_2 nanospheres, due to the pyrolysis of the RF resins during high temperature calcination. The SiO_2 core could be easily dissolved in HF acid to generate hollw carbon spheres and nanopores will be introduced on

HCS shells and graphene sheets, resulting a tiny fraction of broken shells of the HCS. **Figure 2d** comfirmed the uniform hollow structure of the spheres with shell diameter of about 10nm, it also comfirmed the crumpled thin graphene sheets wrapped and interconnected with the HCS to form a 3D hybrid nanostructure. The high resolution TEM image (**Figure S2**) further indicates the coexisting of single- or few- layer graphene sheet in the 3D rGO-HCS hybrid. N_2 adsorption isotherms and pore-size distribution of rGO-HCS are presented in **Figure S3**. The rGO-HCS nanocomposite exhibits a broad pore size distribution from microrange to macrorange with a high BET surface area of 445.07 m^2g^{-1} , confirming the hierarchically porous structure of the 3D rGO-HCS hybrid. In addtion, the total pore volume of the 3D rGO-HCS hybrid is as large as 2.28 cm^3g^{-1}.The hierarchically porous structure with large pore volume would not only prevent sulfur dissolution and shuttling in the electrolyte, but also ensure a high sulfur loading and buffer the volume changes during cycling.

The XRD pattern of the obtained S@rGO-HCS nanocomposite is shown in **Figure S4**,the result demonstrates that the sulfur in the composites exist in the same crystal structure with elemental sulfur (indexed to JCPDS NO. 42-1278). The morphology and structure of 3D S@rGO-HCS nanocomposite was characterized by FESEM. As shown in **Figure 3a**, the sulfur homogeneously dispersed in the rGO-HCS hybrid nanostructure without bulk sulfur observed, furthermore, the 3D interlinked hybrid carbon structure with plentiful nanopores was well-maintained after sulfur impregnation.

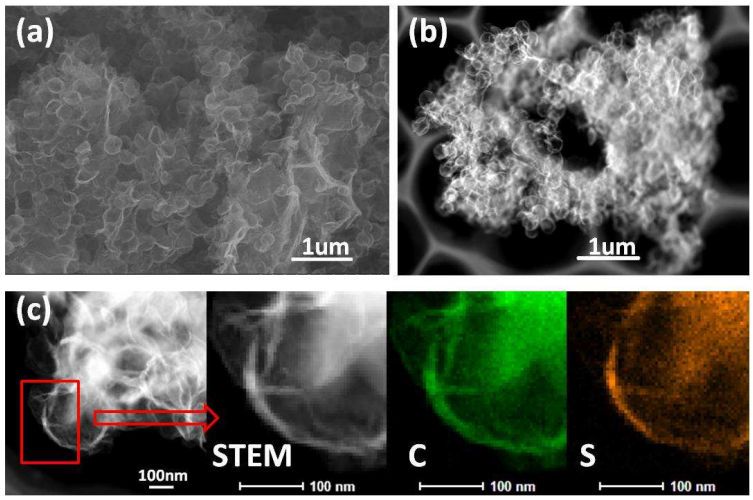

Figure 3 (a) SEM image, (b) STEM image and (c) STEM-EDS elemental maps of S@rGO-HCS nanocomposite

In order to investigate the sulfur distribution in the S@rGO-HCS hybrid nanostructure, scanning transmission electron microscopy (STEM) image and the corresponding elemental mapping were conducted in the selected region (**Figure 3b, c**).From the STEM image of **Figure3b**, we could see that some of the hollow carbon spheres are filled with some bright species and some are filled with nothing, the bright species are believe to be sulfur according to a previously reported article.[50] Because of the electron beam heating effect under the ultra-high vacuum, sulfur may sublimate off from some broken HCSs, leading to hollow carbon shells with nothing left inside. The elemental mapping of carbon and sulfur, in **Figure 3c**, gave visible evidence that the sulfur was homogeously confined within the HCS with a small fraction on the surface of the graphene sheet.These results indicate the sulfur penetrated into the HCSs and also dispersed on the surface of graphene sheets due to the capillarity interaction and good wettability with carbon, on the other hand, the hollow carbon spheres and interlinked graphene networks successfully prohibited the growing up of the sulfur crystals during liquid precipitation process.

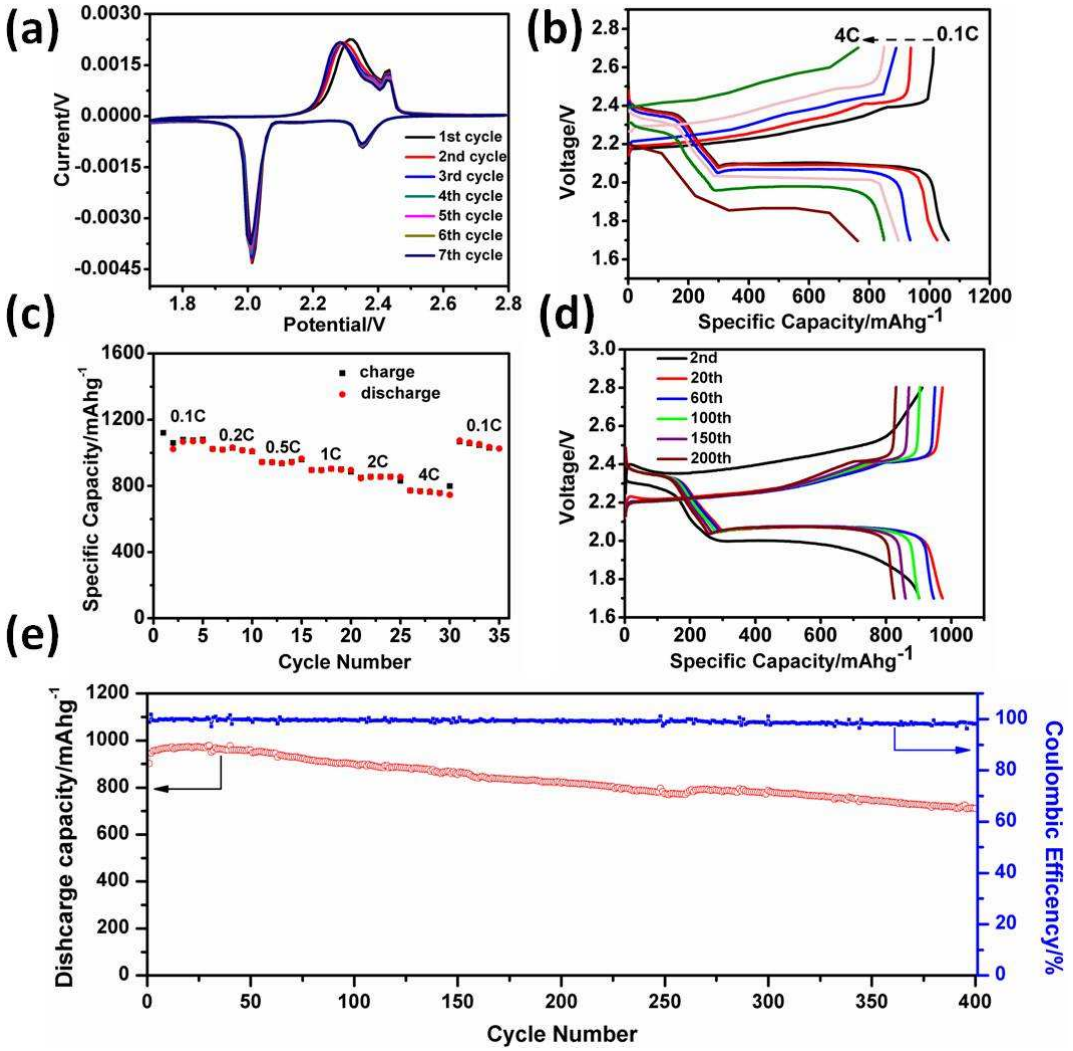

Figure 4 Electrochemical tests of the S@rGO-HCS nanocomposite electrode: (a) Cyclic voltammograms of at a scan rate of 0.1 mV s^{-1}, (b) the charge-discharge curves at different C rates, (c) the rate capability, (d) the charge-discharge curves at different cycles at 0.5C and (e) Cycle performance and the corresponding coulombic efficiency at 0.5C

To test the electrochemical performance of the typical S@rGO-HCS nanocomposite electrode, with a sulfur mass loading of 0.8~1.0 mg cm^{-2}, 2016 type of coin cells were fabricated using lithium foil as the anode and 0.5M lithium bis-trifluoromethanesulfonylimide (LiTFSI) in a mixed solvent of 1,3-dioxolane and 1,2-dimethoxyethane (DOL/DME,1:1,v/v) with 0.5M $LiNO_3$ as the electrolyte. The electrochemical behavior of the S@rGO-HCS nanocomposite electrode was evaluated by cyclic voltammetry (CV) at a scan rate of 0.1mV s^{-1}, the results

were shown in **Figure 4a**. Two well-defined cathodic peaks at 2.35 V and 2.01 V can be assigned to the multistep reduction process of sulfur. The first peak at 2.35 V is attributed to the transformation of cyclo-S_8 to long-chain soluble lithium polysulfides, the second one at 2.01 V is ascribed to the further reduction of those polysulfide species (Li_2S_n, $4 \leq n < 8$) to insoluble short-chain lithium sulfides (Li_2S_n, $n \leq 2$). Two anodic peaks appear at 2.31 V and 2.44 V, respectively, corresponding to the oxidation of the lithium sulfides into long-chain polysulfide and eventually to elemental sulfur. These results agree well with that reported in the literature.[10, 46] It should be noted that except for the little peak shift of the oxidation peak at 2.31 V after the first cycle, the shape and position of the redox and oxidation peaks overlap well for the subsequent 6 cycles, which indicates excellent reversibility and stability of the S@rGO-HCS nanocomposite electrode. The gradual shift of the oxidation peaks around 2.31 V should be ascribed to the gradual activation process of the nanocomposite during cycling, which will also be observed during the charge-discharge tests in the next part.

The rate performance was tested under the galvanostatic mode in the voltage range from 1.7V to 2.8V at discharge-charge rates from 0.1C to 4C (1C=1672 $mAhg^{-1}$). The charge-discharge curves at different C rates and the rate capability of the S@rGO-HCS nanocomposite electrode were shown in **Figure 4b** and **c**. As **Figure 4b** shows these profiles kept similar shapes with low overpotentials observed at different C rates. Even at a high rate of 4C, the curve still exhibited the typical reaction plateaus and delivered a high discharge capacity of ~770 mAh g^{-1}. **Figure 4c** demonstrates the excellent rate capability of the S@rGO-HCS nanocomposite electrode. The discharge specific capacities were stabilized at about 1070, 1010, 940, 900, 850, 770$mAhg^{-1}$ when cycled at 0.1, 0.2, 0.5, 1, 2 and 4C rates, respectively. When the C rate was reduced back to 0.1C, the discharge capacity returned to 1070$mAhg^{-1}$,

indicating excellent reversibility of the S@rGO-HCS nanocomposite electrode. To confirm the advantages of the S@rGO-HCS nanostructure, the S@HCS and S@G composites (**Figure S5**) were also prepared for comparison (Experimental Section). The rate performance of the S@rGO-HCS nanocomposite is obvious better over the S@HCS and S@G composite (**Figure S6)**, which exhibited lower discharge capacities of 580 and 630 $mAhg^{-1}$ at 4C rate, respectively. The superiority of the S@rGO-HCS cathode is probably due to the rational nanostructure design and efficient synthetic method, including the superior electrical conductivity offered by 3D interconnected graphene networks and the homogeneous distribution of nano sulfur confined in the HCS, which facilitate fast electronic/ionic transport and enhance reaction kinetics of sulfur.

The long-term cycling stability of the S@rGO-HCS electrode was also tested at 0.5C rate. It can be seen from **Figure 4d** that except for the discharge/charge curves in the 2nd cycle of the electrode, the profiles of subsequent cycles present stable voltage plateaus and small capacity loss during long cycles. The large overpotential in the 2nd discharge-charge profiles should be ascribed to initial wetting process between cathode material and electrolyte. **Figure 4e** demonstrates the high specific capacity as well as good cycling retention at 0.5C rate. The initial discharge capacity is $901mAhg^{-1}$, and then gradually increases to the highest of 972.6 $mAhg^{-1}$ at 13 cycles, after that, it maintains stable and then shows a slow decay rate during the long cycling. The increase of discharge capacities at initial cycles corresponds to the slow initial activation process of the nanocomposite, which agrees well with the CV results. The capacity retentions are 93.9%, 86.1%, 79.3% and 73.2% after 100, 200, 300 and 400 cycles, respectively. After 400 cycles, the nanocomposite still remained a high capacity of 712 $mAhg^{-1}$ with a low decay rate of 0.052% per cycle. Furthermore, the S@rGO-HCS

nanocomposite electrode shows a high Coulombic efficiency of 98% after the long cycling. The cycling performance of a thicker electrode with sulfur mass loading of 2.0 mg cm^{-2} (Figure S8) was also tested, the discharge capacity of the thicker electrode is about 834 mAh g^{-1} for the first cycle and reaches the highest of 865.2 $mAhg^{-1}$ in the 10th cycle at 0.5C rate, which were slightly lower than that of the typical electrode with sulfur mass loading of 0.8~1.0 mg cm^{-2}. However, the thicker electrode also shows very stable cycle performance with high capacity retention of 93.7% up to 150 cycles. For comparisons, the cyclic stabilities of the S@rGO-HCS, S@HCS and S@G nanocomposite electrodes were tested at 1C rate and illustrated in **Figure S7.** The S@rGO-HCS nanocomposite showed the highest discharge capacity of 897.2 $mAhg^{-1}$ in the 6th cycle (initial discharge capacity is 885.6 $mAhg^{-1}$), with 94.1% capacity retention after 100 cycles. In contrast, the initial discharge capacities of the S@HCS and S@G composite are 701 $mAhg^{-1}$ (reach the highest of 750 $mAhg^{-1}$ in the 13th cycle) and 834.8 $mAhg^{-1}$, respectively, both lower than that of the S@rGO-HCS nanocomposite cathode. Furthermore, the capacity retentions of the S@HCS and S@G are 93.3% and 84.7% after 100 cycles, respectively. Among the three electrodes, the S@rGO-HCS cathode showed the highest discharge capacity and most stable cyclic performance. These results indicate that the design of the S@rGO-HCS nanostructure not only offered fast electronic/ionic transport, but also greatly prevented the dissolution of polysulfides and effectively buffered the volume changes during cycling, thus improved the cycling performance of Li-S batteries.

The suprior comprehensive electrochemical performance should be ascribed to the unique characteristics of the 3D hybrid nanostructure: (1) the 3D conductive graphene networks for rapid electron transfer and robust support; (2) the hierarchical porous space from the hollow

carbon spheres and the 3D interlinked scaffold to buffer the volume changes; (3) homegeous distribution of the nano-sulfur via the solution deposition method; (4) the efficient confinement of the hollow carbon shells and the micropores from the nano hybrids.

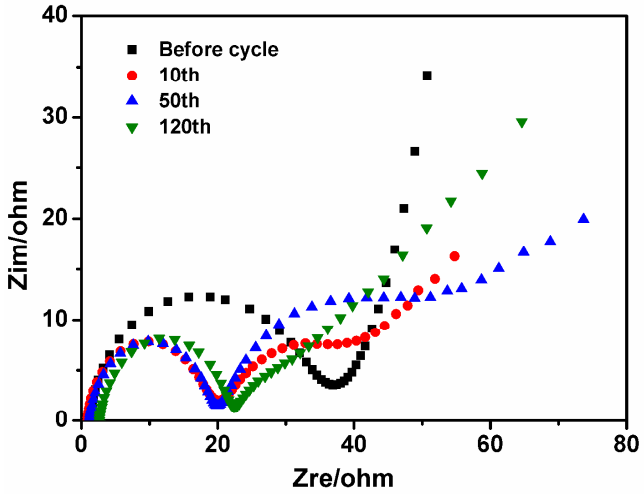

Figure 5 Nyquist plots of the S@rGO-HCS electrode at different cycles at 1C rate

To further understanding of the internal resistance and micro-morphology structure changes of the S@rGO-HCS electrode during long cycling, the Nyquist plots of the cell and post-mortem SEM analysis before and after cycles were performed. **Figure 5** shows the EIS spectra of the S@rGO-HCS electrode at different cycles after fully discharged to 1.7V at 1C rate. The depressed semicircle in the high-frequency region of the plots is related to the solution resistance (R_s) and the charge transfer resistance (R_{ct}) of the cathode, the semicircle in the middle-frequency range could be attributed to the formation of insoluble polysulfide species, and the inclined line in the low-frequency region corresponding to the soluble lithium polysulfide diffusion within the cathode.[56, 57] The R_{ct} of the electrode before cycle is about 38 Ω, it decreases to 20 Ω after 10 cycles during the activation of the electrode, showing faster interfacial charge transfer; after 50 cycles, the R_{ct} almost kept unchanged and it then increased slightly to 23Ω after 120 cycles, confirming the high stability of S@rGO-HCS nanocomposite

during repeated lithiation and delithiation.

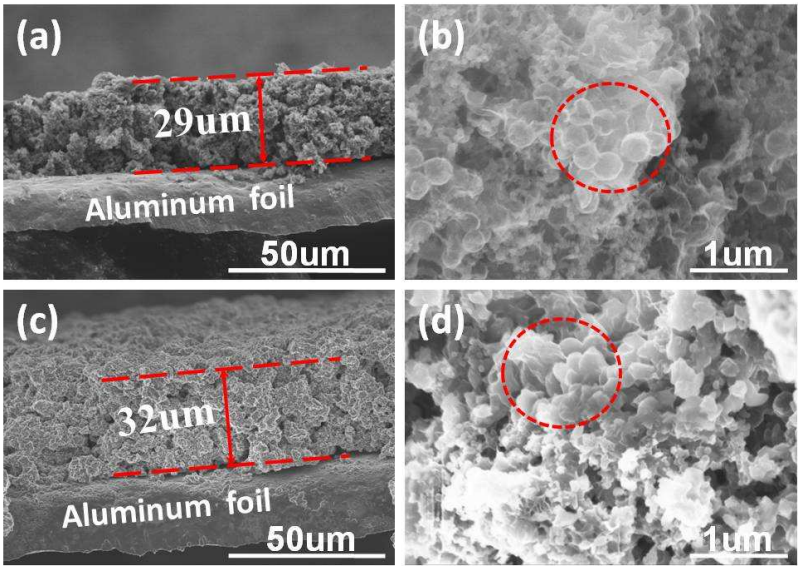

Figure 6 Typical SEM images of the cross sections and corresponding magnified sections of the S@rGO-HCS electrode (a, b) before cycling and (c, d) after 400 cycles

Figure 6 shows the FESEM images of the cross sections of the S@rGO-HCS electrode before cycling and after 400 cycles. The morphology of the fresh electrode were shown in **Figure 6a** and magnified in **Figure 6b.** The cathode structure of the fresh electrode shows a thickness of ~29um with porous structures homogenously interconnected with each other, the magnified SEM image indicates the Super P carbons homogenously distributed among the S@rGO-HCS nanostructures. After 400 cycles, the cathode demonstrates a more compact nanostructure with fewer pores than that of the fresh electrode with a thickness of ~32um (**Figure 6c**).The thickness of the cathode changed by ~10% after 400 cycles due to the repetitive conversion of sulfur to polysulfides and Li_2S, much lower than the theoretical expansion of 80% and thickness variation of 22% after only one cycle reported previously. [5] Furthermore, the integrity of the electrode has been well maintained without structural destruction. The smooth nano-spheres in the magnified image in **Figure 6d** indicates polysulfides and L_2S species fully filled in the HCS, and the discharge products are homogeneously distributed among the

S@rGO-HCS network without aggregates observed. The results not only indicate that the nano-sized sulfur are uniformly dispersed among the S@rGO-HCS nanostructure during the solution precipitation process, but also reveal the 3D interlinked networks with large porosity could effectively buffer the large volume change and maintain the structural integrity. As previous study [55] indicates, electrode homogeneity and integrity play important roles in ensuring good performance for lithium sulfur batteries. The 3D rGO-HCS framework with hierarchical porous structure design could effectively achieve these goals, showing promising potentials of the S@rGO-HCS nanocomposite as high-performance Li-S battery cathode, in terms of the execellent cycling performance, suprior rate capability and high Coulombic efficiency.

3 Conclusion

In conclusion, a novel nanostructured 3D rGO-HCS hybrid was fabricated via hydrothermal self-assembly method using GO and RF@SiO_2 spheres as precusors.The graphene sheets and hollow carbon spheres were in situ interconnected with each other, building a conductive and robust 3D network with hierarchical porous structure. The novel 3D carbon hybrid is used to encapsulate nano-sulfur via solution depositon method as cathode material for Li-S batteries. Such rational nanostructure design are favorable for fast electron and ion transportion, succesfull maintenance of structural integrity and efficient confinement of polysulfide dissolution and shuttling. The synergic effects from the 3D carbon-network design leads to execellent comprehensive performance, which is superior to that of the hollow spheres or graphene based sulfur cathode reported in recent years (Supporting Informantion Table S1). High discharge capacities of ~1070 $mAhg^{-1}$, ~1010$mAhg^{-1}$, ~940 $mAhg^{-1}$,~900 $mAhg^{-1}$,~850 $mAhg^{-1}$ and ~770 $mAhg^{-1}$ can be achieved at 0.1C, 0.2C , 0.5C , 1C , 2C and 4C, respectively.

Furthermore,a low capacity decay rate of 0.052% with an excellent Coulombic efficiency of 98.8% was retained after 400 cycles at 0.5C. In addition to Li-S batteries, the 3D rGO-HCS nanostructure could also be applied in other energy storage and conversion field, such as other lithium batteries, supercapcitors, catalysis,in which fast electron transport and structural flexibility is critical.

4 Experimental Section

Synthesis of RF@SiO_2 spheres and GO: RF@SiO_2 nanospheres were synthesized by a stöber method, modifying a previously reported method. [58] Briefly, 9.6 ml ammonia aqueous solution (25 wt%) was mixed well with a solution containing 144ml ethanol and 96ml DI water, then 12ml tetraethylorthosilicate (TEOS) mixed with 48 ml ethanol was added into the above solution under magnetic stirring for 10 min. Subsequently, 1.44 g resorcinol and 2.12 g formaldehyde solution was then added to the reaction solution and stirred for 24 h at room temperature. Finally, the reaction solution was heated for 24 h at 100°C in a sealed autoclave followed by centrifugation and air drying. GO was prepared from graphite flakes by an improved Hummers method. [59] A homogeneous graphene oxide aqueous dispersion (10.0 mg ml^{-1}) was sonicated for 2 h before use.

Preparation of 3D rGO-HCS hybrid and HCS: First, 1.5g RF@SiO_2 nanoparticles were dispersed in 60ml water and sonicated for 3h, then 30ml GO aqueous solution (10.0 mg ml) was added in and stirred for 1h, after that, 0.88g ascorbic acid dissolved in 40ml water was added, finally the mixed solution was heated for 12h at 180°C in an sealed autoclave to form a 3D GO-RF@SiO_2 gel. The gel was dried in a vacuum oven at 60°C for 12h and then heated to 900°C for 2h under N_2 atmosphere, followed by etching of 10wt% HF solution to generate 3D

rGO-HCS nanocomposite. For comparison, the RF@SiO_2 nanoparticles were also heated to 900°C for 2h under N_2 atmosphere, followed by etching of 10wt% HF solution to obtain HCS nanocomposite.

Preparation of S@rGO-HCS, S@HCS and S@G nanocomposite: The S@rGO-HCS nanocomposite was fabricated via an in-situ solution deposition method. Breifly, 0.05 g 3D rGO-HCS nanocomposite was added into aqueous-ethanol (80 ml: 20 ml) solution and sonicated for 1h, then 1.0g $Na_2S{\cdot}9H_2O$ and 0.81g Na_2SO_3 were dissovled in 50 ml DI water and poured into the above solution.Then 20 ml 1M hydrochloric acid solution and 6 mg PVP was added in under magnetic stir for 1 h. Finally, the reaction solution was ultrasonicated for 30 min and centrifuged 3 times with DI water, after vacuum drying at 60°C for 12 h, the S@rGO-HCS nanocomposite was obtained. For comparisons, the S@HCS and S@G nanocomposite were prepared following the same procedure as that of S@rGO-HCS composite, but replacing the rGO-HCS with HCS or G (graphene sheets purchased from Ningbo Morsh Technology. Co., Ltd.).The sulfur contents in the as-prepared composites were also calculated by the mass change before and after the formation of the composite, which almost agree with TG analysis (Figure S9). The sulfur contents in the S@rGO-HCS, S@HCS and S@G nanocomposite were 65wt%, 65wt% and 67.7wt%, respectively.

Materials Characterization: The structure of HCS, rGO-HCS and S@rGO-HCS materials were measured by XRD (SIEMENS D-500) using Cu Ka radiation, ranging from 10° to 60° at a step of $8°min^{-1}$. The micro morphologies of the nanocomposite were studied using field emission scanning electron microscope (HITACHI S4800, Japan). TEM, HRTEM images, and STEM-EDS elemental mapping were recorded with a FEI Tecnai 2100 instrument. The nitrogen adsorption-desorption analysis was done at 77.3 K on a V-Sorb 2800 equipment. The

thermogravimetric analysis (TGA) was measured with a TGA-600 with a heating rate of 10□min^{-1} under N_2 atmosphere to confirm the sulfur content in the composite.

Electrochemical characterizations: Electrochemical experiments were performed using 2016 type coin cells. The working electrode was prepared by mixing 80 wt% sulfur cathode materials with 12 wt% Super P and 8 wt% LA133 aqueous binder using water and isopropanol as the solvent. After mixing well, the slurry was pasted on Al foil and dried overnight at 60℃ in a vacuum oven. 0.5M lithium bis-trifluoromethanesulfonylimide (LiTFSI) in a mixed solvent of 1,3-dioxolane and 1,2-dimethoxyethane (DOL/DME, 1:1, v/v) with 0.5M $LiNO_3$, purchased from Fosai New Material Co., Ltd (Suzhou), was used as electrolyte, lithium metal foil was used as the anode and the polypropylene membranes from Celgard Inc. were used as the separators. The typical mass loading of sulfur is about 0.8~1.0 mg cm^{-2}.Galvanstatic charge-discharge measurements were performed using a battery tester (LAND CT-2001A, Wuhan, China) at room temperature in a potential range of 1.7~2.8 V (vs. Li+/Li) at current densities of 0.1C, 0.2C, 0.5C, 1C, 2C, 4C (1C=1672 mA h g^{-1}). Cyclic voltammetry (CV) was performed with an electrochemical workstation (CHI 660 C) between 1.7 and 2.8V at a sweep rate of 0.1 mV s^{-1}. Electrochemical Impedance (EIS) analyses were conducted using the same equipment from 100 kHz to 100 mHz.

Acknowledgements

The authors acknowledge the Aid program for Science and Technology Innovative Research Team in Higher Education Institutions for Hunan Province.

[1] Y. Yang , G. Zheng , Y. Cui , *Chem. Soc. Rev.* **2013** , 42 , 3018 .

[2] A. Manthiram, Y. Fu, Y.-S. Su, *Acc. Chem. Res.* **2013**, 46, 1125.

[3] S. Evers, L. F. Nazar, *Acc. Chem. Res.* **2013**, 46, 1135.

[4] Y.-X. Yin, S. Xin, Y.-G. Guo, L.-J. Wan. *Angew. Chem. Int. Ed.* **2013**, 52, 13186-13200

[5] S. E. Cheon, S. S. Choi, J. S. Han, Y. S. Choi, B. H. Jung, H. S. Lim, *J. Electrochem. Soc.* **2004**, 151, A2067.

[6] Y. V. Mikhaylik, J. R. Akridge, *J. Electrochem. Soc.* **2004**, 151, A1969.

[7] H.Yamin, A. Gorenshtein, J. Penciner, Y. Sternberg, E. Peled, *J. Electrochem. Soc.* **1988**, 135, 1045.

[8] E. Peled, T. Sternberg, A. Gorenshtein, Y. Lavi, *J. Electrochem. Soc.* **1989**, 136, 1621.

[9] Z. W. Seh, W. Y. Li, J. J. Cha, G. Y. Zheng, Y. Yang, M. T. McDowell, P. C. Hsu, Y. Cui, *Nat.Commun.* **2013**, 4, 1331.

[10] L. Xiao, Y. Cao, J. Xiao, B. Schwenzer, M. H. Engelhard, L. V. Saraf, Z. Nie, G. Exarhos, J. Liu, J. *Adv. Mater.* **2012**, 24, 1176.

[11] W. Zhou, Y. Yu, H. Chen, F. J. DiSalvo, H. D. Abruña, *J. Am.Chem.Soc.*2013, 135 (44), 16736.

[12] L. Yin, J. Wang, F. Lin, J. Yang, Y. Nuli, *Energy Environ. Sci.* **2012**, 5, 6966.

[13] T. H. Hwang, D. S. Jung, J. S. Kim, B. G. Kim, J. W. Choi, *Nano Lett.* **2013**, 13, 4532.

[14] W. Li, Q. Zhang, G. Zheng, Z. W. Seh, H.Yao, Y. Cui. *Nano Lett.* **2013**, 13, 5534.

[15] Y.-S. Su, A. Manthiram, *Chem. Commun.* **2012**, 48, 8817.

[16] Y.S. Su, A. Manthiram, *Nat. Commun.* **2012,** 3, 1166.

[17] Y.-J. Choi, Y.-D. Chung, C.-Y. Baek, K.-W. Kim, H.-J. Ahn, J.-H. Ahn, *J. Power Sources,* **2008**,184, 548-552.

[18] X. Wang, Z. Wang, L. Chen. *J. Power Sources.* **2013***,* 242, 65-69

[19] S. C. Han, M. S. Song, H. Lee, H. S. Kim, H. J. Ahn, J. Y. Lee, *J. Electrochem. Soc.*

2003,150,A889.

[20] J. J. Chen, X. Jia , Q. J. She, C. Wang, Q. Zhang , M. S. Zheng , Q. F. Dong , *Electrochimica Acta.* **2010** , 55 , 8062.

[21] J. Guo , Y. Xu , C. Wang , *Nano Lett.* **2011** , 11 , 4288 .

[22] S. Dörfl er , M. Hagen , H. Althues , J. Tübke , S. Kaskel ,M. J. Hoffmann , *Chem. Commun.* **2012** , 48 , 4097.

[23] G. M. Zhou , D. W. Wang , F. Li , P. X. Hou , L. C. Yin , C. Liu ,G. Q. Lu , I. R. Gentle , H. M. Cheng , *Energy Environ. Sci.* **2012**, 5, 8901.

[24] K. K. Jin, X. F. Zhou, L. Z. Zhang, X. Xin, G. H. Wan, Z. P. Liu, *J. Phys. Chem. C* **2013**, 117, 21112.

[25] X. Ji, K. T. Lee , L. F. Nazar , *Nat. Mater.* **2009**, 8,500.

[26] C. Liang , N. J. Dudney , J. Y. Howe , *Chem. Mater.* **2009**,21,4724.

[27] G. He, X. Ji, L. Nazar, *Energy Environ. Sci.* **2011**, 4, 2878.

[28] X. Y. Tao ,X. R. Chen , Y. Xia , H. Huang , Y. P. Gan , R. Wu , F. Chen , W. K. Zhang , *J. Mater. Chem. A* **2013**,1, 3295.

[29] T. Xu , J. X. Song , M. L. Gordin ,H. Sohn , Z. X. Yu , S. R. Chen , D. H. Wang , *ACS Appl. Mater. Interfaces* **2013**,5,11355.

[30] D. Li , F. Han , S. Wang , F. Cheng , Q. Sun , W. C. Li , *ACS Appl. Mater. Interfaces* **2013,** 5, 2208.

[31] J. Wang, Y.-S. He, J. Yang. *Adv. Mater.* **2014**, 3,569.

[32] C. X. Zu, A. Manthiram, *Adv. Energy Mater.* **2013**, 3, 1008.

[33] G. Ma, Z. Wen, J. Jin, Y. Lu, X. Wu, M. Wu, C. Chen. J. Mater. Chem. A, 2014, 2, 10350.

[34] H. Xu, Y. Deng, Z. Shi, Y. Qian, Y Meng, G. Chen. J. Mater. Chem. A, 2013, 1,15142

[35] H. Wang, Y.Yang, Y. Liang, J. T. Robinson, Y. Li, A. Jackson, Y. Cui, H. Dai, *Nano Lett.* **2011**, 11, 2644.

[36] S. Evers, L. F. Nazar, *Chem.Commun.* **2012**,48,1233.

[37] Y. Qiu, W. Li,W. Zhao, G. Li, Y. Hou, M. Liu, L. Zhou, F. Ye, H. Li, Z. Wei, S. Yang, W. Duan, Y. Ye, J. Guo, Y. Zhang. *Nano Lett.* **2014**, 14 (8), 4821.

[38] C. Tang , Q. Zhang ,M.-Q. Zhao , J.-Q.Huang , X.-B. Cheng ,G.-L.Tian , H.-J. Peng , F.Wei. *Adv. Mater.* **2014**, 26(35),6100.

[39] L. W. Ji, M. M. Rao, H. M. Zheng, L. Zhang, Y. C. Li, W. H. Duan, J. H. Guo, E. J. Cairns, Y. G. Zhang, *J. Am. Chem. Soc.* **2011**,133, 18522.

[40] S. Liu, K. Xie,Y. Li, Z. Chen, X. Hong, L. Zhou, J.Yuan, C. Zheng, *RSC Adv.* **2015**, 5, 5516.

[41] J. Rong, M. Ge, X. Fang, C. Zhou. *Nano Lett.* **2014**, 14, 473.

[42] C. Wang, K. Su, W. Wan, H. Guo, H. H. Zhou, J. T. Chen, X. X. Zhang, Y. H. Huang, *J. Mater. Chem. A* **2014**, 2, 5018.

[43] G. Y. Zheng , Y. Yang , J. J. Cha , S. S. Hong , Y. Cui , *Nano Lett.* **2011**, 11, 4462.

[44] L. W. Ji , M. M. Rao , S. Aloni , L. Wang , E. J. Cairns ,Y. G. Zhang , *Energy Environ. Sci.* **2011**, 4, 5053.

[45] R. Elazari ,G. Salitra , A. Garsuch , A. Panchenko , D. Aurbach , *Adv. Mater.* **2011** ,23 , 5641 .

[46] N. Jayaprakash, J. Shen, S. S. Moganty, A. Corona, L.A. Archer, *Angew. Chem., Int. Ed.* **2011**, 50, 5904.

[47] C. Zhang, H. Wu, C. Yuan, Z. Guo, X. W. Lou, *Angew. Chem., Int. Ed.* **2012**, 51, 9592.

[48] N. Brun, K. Sakaushi, L. H. Yu, L. Giebeler, J. Eckert, M. M. Titirici, *Phys. Chem. Chem. Phys.* **2013**,15, 6080.

[49] G. He, S. Evers, X. Liang, M. Cuisinier, A. Garsuch, L. F. Nazar, *ACS Nano* **2013**, 7, 10920.

[50] W. Zhou, X. Xiao, M. Cai, L. Yang, *Nano Lett.* **2014**, 14, 5250−5256.

[51] Z.Wang, X. Li, Y. Cui, Y. Yang, H. Pan, Z. Wang, G. Qian, *J.Electrochem.Soc*.**2014**,161 (9) ,1231.

[52] J. Tang, J. Yang , X. Zhou, *RSC Adv.*, 2013,3,16936.

[53]X. Yang, L. Zhang, F. Zhang, Y. Huang, Y. Chen, *ACS Nano* **2014**, 8 (5), 5208.

[54]X. Chen , Z. Xiao , X. Ning , Z. Liu , Z.Yang , C. Zou , S. Wang ,X. Chen , Y. Chen , S. Huang. *Adv. Energy Mater.* **2014**, 1301988.

[55] R.Elazari, G. Salitra, Y. Talyosef, J. Grinblat,C.S.-Kelley, A. Xiao, J. Affinitob, D. Aurbach, *J. Electrochem. Soc.* **2010**,157,A1131.

[56] L. Yuan, X. Qiu, L. Chen, W. Zhu, *J. Power Sources* **2009**, 189, 127.

[57] W. Li, G. Zheng, Y. Yang, Z. W. Seh, N. Liu, Y.Cui, *Proc. Natl. Acad. Sci. U.S.A.* **2013**,110, 7148.

[58] A. B. Fuertes, P. Valle-Vig´on, M. Sevilla, *Chem. Commun.*, **2012**, 48, 6124–6126.

[59] D. C. Marcano, D. V. Kosynkin, J. M. Berlin, A. Sinitskii,Z. Z. Sun, A. Slesarev, L. B. Alemany, W. Lu , J. M. Tour, *ACS Nano* **2010**, 4, 4806.

Graphical Abstract

3D Graphene interconnected with Hollow Carbon Sphere Framework as High Performance Cathode Material for Lithium Sulfur Batteries

Shuangke Liu,[a] Kai Xie,[a] Zhongxue Chen,[a b] Yujie Li,[a] Xiaobin Hong,[a] Jing Xu,[a] Liangjun Zhou,[a] Junfei Yuan[a] and Chunman Zheng*[a]*

A novel 3D rGO-HCS Framework was designed via hydrothermal self-assembly method. When used as sulfur cathode， the obtained S@rGO-HCS composite delivers a low capacity-decay rate of 0.052% per cycle after 400 cycles and shows high rate performance with ~770 mA h g^{-1} at 4C rate. The superior comprehensive electrochemical performance is ascribed to the synergic effects from the novel 3D graphene-network design.